Strain Effect in Semiconductors

Yongke Sun • Scott E. Thompson • Toshikazu Nishida

Strain Effect in Semiconductors

Theory and Device Applications

Yongke Sun
SanDisk Corporation
601 McCarthy Boulevard
Milpitas, CA 95035
USA
Yongke.Sun@sandisk.com

Scott E. Thompson
University of Florida
Department Electrical & Computer Engineering
Gainesville, FL 32611
535, Engineering Bldg.
USA
thompson@ece.ufl.edu

Toshikazu Nishida
University of Florida
Department Electrical & Computer Engineering
223 Benton Hall
Gainesville FL 32611-6200
USA
nishida@ufl.edu

ISBN 978-1-4419-0551-2 e-ISBN 978-1-4419-0552-9
DOI 10.1007/978-1-4419-0552-9
Springer New York Dordrecht Heidelberg London

Library of Congress Control Number: 2009938434

© Springer Science+Business Media, LLC 2010
All rights reserved. This work may not be translated or copied in whole or in part without the written permission of the publisher (Springer Science+Business Media, LLC, 233 Spring Street, New York, NY 10013, USA), except for brief excerpts in connection with reviews or scholarly analysis. Use in connection with any form of information storage and retrieval, electronic adaptation, computer software, or by similar or dissimilar methodology now known or hereafter developed is forbidden.
The use in this publication of trade names, trademarks, service marks, and similar terms, even if they are not identified as such, is not to be taken as an expression of opinion as to whether or not they are subject to proprietary rights.

Printed on acid-free paper

Springer is part of Springer Science+Business Media (www.springer.com)

Contents

1 Overview: The Age of Strained Devices 1
1.1 Origin of the Strained-Si Technology 1
1.2 Strain in Semiconductor Devices 1
1.2.1 Conventional Simple Scaling 2
1.2.2 Feature-Enhanced CMOS 2
1.2.3 Variable Strain Sensors 4
1.2.4 Strained Quantum Well Optoelectronics 4
1.3 Organization 5

Part I Band Structures of Strained Semiconductors

2 Stress, Strain, Piezoresistivity, and Piezoelectricity 9
2.1 Strain Tensor 9
2.2 Stress Tensor 11
2.3 Elastic Compliance and Stiffness Constants 14
2.4 Examples of Stress–Strain Relations 16
2.4.1 Hydrostatic and Shear Strain 18
2.5 Piezoresistivity 19
2.6 Piezoelectricity 20

3 Strain and Semiconductor Crystal Symmetry 23
3.1 Introduction 23
3.2 Symmetry and Strain: Overview 24
3.2.1 Examples of Crystal Lattices 24
3.2.2 Crystal Symmetry 26
3.2.3 Energy Band Symmetry 27
3.2.4 Strain Effects on Energy Bands 30
3.3 Symmetry Effects in Determining Electronic States 34
3.3.1 Translational Symmetry and Reciprocal Space 35
3.3.2 Bloch Theorem 37
3.3.3 Point Symmetry Effects on Electronic States 38

3.4 Semiconductor Crystal Classes and Systems . . . 41
3.4.1 Crystal Classes and Systems . . . 41
3.4.2 Cubic Semiconductors . . . 43
3.5 Strain Effects on Electronic Band Structures . . . 45
3.5.1 Evolution of Crystal Systems with Strain . . . 45
3.5.2 Strained Band Structures . . . 47
3.6 Summary of Symmetry, and Its Limitation . . . 49

4 Band Structures of Strained Semiconductors . . . 51
4.1 Introduction . . . 51
4.2 Strain Effects on Semiconductor Band Structures: A Qualitative Overview . . . 52
4.2.1 Tight-Binding Formation of Semiconductor Crystals . . . 53
4.2.2 Overlap Integrals . . . 56
4.2.3 Properties of Electronic Wave Functions . . . 58
4.2.4 Strain Effects on Tight-Binding Band Structures . . . 61
4.2.5 Determining Deformation Potentials Using Tight-Binding Method . . . 63
4.2.6 Summary for the Qualitative Overview . . . 64
4.3 Brief Introduction to Plane Wave Expansion Method . . . 64
4.4 Tight-Binding Method . . . 67
4.4.1 A General Introduction . . . 67
4.4.2 The sp^3 Tight-Binding Model . . . 72
4.4.3 Tight-Binding Band Structure . . . 76
4.4.4 The sp^3 Hybridization and Bond Orbital Approximation . . . 82
4.5 Strain Effects in Tight-Binding Framework . . . 84
4.5.1 Hydrostatic Strain: d^{-2} Principle . . . 84
4.5.2 Shear Strain: Bond Rotation . . . 87
4.6 Summary for the Tight-Binding Method . . . 89
4.7 The $k \cdot p$ Method . . . 90
4.7.1 Effective Mass . . . 90
4.7.2 $k \cdot p$ Hamiltonian . . . 92
4.7.3 Single Band Perturbation Expansion . . . 93
4.7.4 Degenerate Band Perturbation Expansion . . . 96
4.8 Luttinger Hamiltonian . . . 98
4.8.1 Luttinger Hamiltonian Without Spin–orbit Coupling . . . 98
4.8.2 Luttinger Hamiltonian with Spin–Orbit Coupling . . . 100
4.8.3 4×4 Analytical Energy Dispersion . . . 103
4.8.4 Coordinate Transformation . . . 104
4.9 Kane's Model with Remote Band Coupling . . . 105
4.10 Band Structure of Selected Semiconductors . . . 107
4.11 Density of States and Conductivity Mass . . . 112
4.12 Pikus–Bir Strain Hamiltonian . . . 118

4.13 Strained Band Structures 124
4.13.1 Conduction Band 124
4.13.2 Analytical Results for Valence Bands with 4×4 Hamiltonian 127
4.13.3 Valence Bands of Strained Semiconductors with Split-Off Band Coupling 130
4.13.4 Band Gap Shift with Strain 133

5 Low-Dimensional Semiconductor Structures 137
5.1 Introduction 137
5.2 Overview: Low-Dimensional Semiconductor Structures 138
5.2.1 MOS Structure and MOSFET Channel 139
5.2.2 Heterojunction 140
5.2.3 Square Quantum Well 142
5.2.4 Nanowire 144
5.3 Electronic Properties of Low-Dimensional Structures 145
5.3.1 Envelope Function Theory 145
5.3.2 Triangular Potential Well Approximation 148
5.3.3 Quantum Well and Quantum Wire Band Structures . . . 151
5.3.4 P-Type Structures 152
5.3.5 2D and 1D Density of States 153
5.4 Self-Consistent Calculation 155
5.4.1 Self-Consistent Procedure 156
5.4.2 Variational Method 157
5.4.3 Finite Difference Method 160
5.5 Subband Structures of 2D Electron/Hole Gas 164
5.5.1 Self-Consistent Confining Potential 164
5.5.2 Charge Distribution vs. Material 166
5.5.3 Subband Structure in GaAs/AlGaAs Heterostructures . 167
5.5.4 Subband Structure in Square Quantum Wells 170
5.5.5 Subband Energy vs. Well Width 172
5.5.6 In-Plane Energy Dispersion 173
5.6 Strain Effects on Subband Structures 176
5.6.1 GaAs Conduction Band 176
5.6.2 Si Conduction Band 179
5.6.3 Valence Band 180

Part II Transport Theory of Strained Semiconductors

6 Semiconductor Transport 185
6.1 Introduction 185
6.2 Carrier Transport: A Qualitative Overview 185
6.2.1 Drude's Electron Transport Model 186

6.2.2 Strain Effects on Electron/Hole Transport in MOSFETs 187
6.3 Scattering in Semiconductors: General Consideration 190
6.3.1 Scattering Rate 190
6.3.2 Momentum Relaxation Rate 192
6.4 Scattering Processes in Semiconductors 193
6.4.1 Lattice Scattering 193
6.4.2 Acoustic Phonon Scattering 195
6.4.3 Piezoelectric Scattering 196
6.4.4 Optical Phonon Scattering 197
6.4.5 Polar Optical Phonon Scattering 198
6.4.6 Impurity Scattering 200
6.5 Boltzmann Equation 202
6.5.1 Electron Conductivity Mass of Si 205
6.6 New Features in 2D Scattering 208
6.6.1 Broken Symmetry due to Confinement 208
6.6.2 Surface Roughness Scattering 210
6.7 Strain Effects on Carrier Transport 214
6.7.1 Piezoresistance 214
6.7.2 Electron Transport 216
6.7.3 Hole Transport 221
6.7.4 Strain on Surface Roughness Scattering 223
6.7.5 Transport in High Effective Field 225
6.7.6 Strain Effects in Ballistic Transport Regime 231

Part III Strain in Semiconductor Devices

7 Strain in Electron Devices 235
7.1 Strain-Si Technology 235
7.2 Strained Electron Devices 239
7.2.1 Strained Planar MOSFETs 239
7.2.2 Strained Si-on-Insulator (SOI)/SiGe-on-Insulator (SGOI) Devices 241
7.2.3 Strain in Other Electron Devices 244
7.3 Strain Enhanced Mobility 244
7.4 SiGe Devices 251
7.5 Leakage and Reliability of Strained-Si 255
7.5.1 Strain on Threshold Voltage 255
7.5.2 Leakage Current in Strained-Si Devices 257
7.5.3 Reliability of Strained-Si 259
7.6 Defects in Strained-Si 261
7.7 Scalability of Strain 264

8 Piezoresistive Strain Sensors ... 267
8.1 Introduction ... 267
8.2 Resistor as Discrete Strain Transducer ... 268
8.2.1 Gauge Factor ... 269
8.2.2 Piezoresistance ... 270
8.2.3 Coordinate Transformation to Arbitrary Directions ... 273
8.3 Integrated Piezoresistive Stress Transducers ... 281
8.3.1 Canonical Cantilever-Based Piezoresistive Force Transducer ... 282
8.3.2 Circular Diaphragm MEMS Piezoresistive Microphone ... 288

9 Strain Effects on Optoelectronic Devices ... 291
9.1 Introduction ... 291
9.2 Strain Effects in Optoelectronic Devices: An Overview ... 292
9.2.1 Photon Emission and Absorption ... 292
9.2.2 Working Principles for Photodiodes and Quantum Well Lasers ... 294
9.2.3 Strain Applications in Optoelectronic Devices ... 298
9.3 Optical Processes in Semiconductors ... 306
9.3.1 Light Absorption Coefficient ... 306
9.3.2 Joint Density of States ... 311
9.3.3 Optical Transitions in Quantum Wells ... 313
9.3.4 Optical Matrix Elements ... 314
9.4 Nonequilibrium Carrier Distribution and Gain ... 317
9.5 Strained Quantum Well Lasers ... 321
9.5.1 Subband Structure and Modal Gain ... 321

Appendix: Effective Mass Theorem ... 327

References ... 331

Index ... 347

Preface

Strain is an old concept in semiconductor physics. However, strain applied in Si logic technology is a relatively new response to the diminishing returns of pure geometric scaling. Process-induced strain was the first additive feature enhancement introduced into planar Si MOSFET transistors by Intel in 2002 which heralded a new age of feature enhanced CMOS scaling. Prior to strain in logic technologies, Si and Ge piezoresistive strain sensors were initiated much earlier, circa 1957, to respond to variable strain. Strain has also been used to enhance optoelectronic devices such as quantum well lasers incorporated via lattice-mismatched heterostructures. Before the advent of strain enhanced MOSFETs, there were already many, though scattered, research reports on strain effects in semiconductors. However, there had not been a strong driving force for strain studies in semiconductors until it began to play a major role in the mainstream VLSI semiconductor industry. Now in almost every semiconductor workshop, strain is induced by various means to boost device performance. Device and process engineers apply advantageous strain to improve electronic product performance and power at low additive cost to meet the demand of consumers.

There are excellent books on strain physics, such as Symmetry and Strain-induced Effects in Semiconductor by Pikus and Bir, and also many books on device physics, such as Fundamentals of Solid-State Electronics by Sah and Physics of Semiconductor Devices by Sze, as well as numerous papers published on the topic of strained Si, Ge, and other semiconductors, but there is a lack of a single text that combines both strain and device physics. Therefore, drawing from our experience both in the semiconductor industry and in the academic field, we have attempted to summarize in this book some of the latest efforts to reveal the physics underlying the advantages that strain has brought forth as well as its applications in devices, and perhaps help guide the development of strained semiconductor devices. Thus in this book, we have included much of our own research, and have collected many valuable achievements and ideas by the research community. However, due to space

constraints, we note that unfortunately only representative papers and not all key papers have been cited in this work.

This book is designed for two levels of readers. For readers such as students and applications engineers who seek a qualitative discussion, we provide a qualitative overview at the beginning of every chapter. For advanced graduate students and research and development engineers with a background in semiconductor physics who wish to dig deeper, the second part of each chapter provides a more systematic and mathematically involved treatment of the subject. We hope this book provides useful insight into the common physics of strain effects in semiconductors that serve as the foundation for the varied strained semiconductor device applications for both sets of readers.

1

Overview: The Age of Strained Devices

1.1 ORIGIN OF THE STRAINED-SI TECHNOLOGY

One of the predecessors of strained Si to enhance MOSFET performance is the research that showed enhanced electron mobilities in n-type (100) $Si/Si_{1-x}Ge_x$ multilayer heterostructures and hole mobilities in p-type (100) $Si/i\text{-}Si_{1-x}Ge_x/Si$ double-heterostructures in the early 1980s (Manasevit et al, 1982; R.People et al, 1984). Strain caused by the lattice mismatch was suspected as one of the factors for the mobility enhancement. The physical mechanism for the enhancement can be traced back to the theoretical formulation of deformation potentials by Bardeen and Shockley (Bardeen and Shockley, 1950; Shockley and Bardeen, 1950) in 1950 and the experimental measurements of the piezoresistance effect, a change in resistance with mechanical stress, by Smith (Smith, 1954).

In an era of rapidly changing technology, strain is a relatively old topic in semiconductor physics, yet its tangible effects on band structure and carrier transport have spurred a renewed interest in strained semiconductor physics. To model lattice scattering, deformation potential theory was developed by Bardeen and Shockley to characterize the band energy shift with strain caused by phonons (Bardeen and Shockley, 1950; Shockley and Bardeen, 1950). Herring and Vogt (Herring and Vogt, 1956) then extended deformation potentials to model transport in strained semiconductors. Deformation potential theory is still the primary method to model the band shift and warping in energy band calculations (Oberhuber et al, 1998; Fischetti and Laux, 1996).

1.2 STRAIN IN SEMICONDUCTOR DEVICES

While strain physics is fundamental, the source of strain is technology and device dependent. For example, strain can result from phonon-induced lattice vibrations in homogeneous semiconductors, lattice-mismatched film growth

Y. Sun et al., *Strain Effect in Semiconductors: Theory and Device Applications*, DOI 10.1007/978-1-4419-0552-9_1,
© Springer Science+Business Media, LLC 2010

in epitaxial heterostructures, intrinsic stress in deposited thin films, and applied external stress. Prior to the development of heteroepitaxy and chemical vapor deposition, variable strain transducers were developed to exploit the piezoresistive effect in Si and Ge to construct strain gauges and stress transducers (Mason and Thurston, 1957; Burns, 1957) that responded to different values of strain or stress. With the advent of micromachining, more elaborate piezoresistive transducers have been fabricated using microelectromechanical systems (MEMS) technology. Simultaneously, integrated circuits were invented and evolved exponentially in density and performance along the path portended by Moore's law through improvements in lithography and microelectronics fabrication technologies until various obstacles began to loom. Finally, continual geometric scaling of the metal-oxide-semiconductor field-effect transistor (MOSFET) channel length, gate dielectric thickness, and junction depth led to increasing off-state channel leakage, gate leakage, source–drain resistance, and short-channel effects. Performance improvement at each technology node by simple geometrical scaling became more problematic and costly until the end of simple scaling for CMOS was predicted.

1.2.1 Conventional Simple Scaling

The end of simple scaling for a solid state device technology is not new. Scaling of silicon bipolar junction transistors (BJT) ended in the 90s for various reasons including voltage, base width, and power density limits. However, the unrelenting scaling of the competing complementary MOS (CMOS) as another factor cannot be overestimated. By the mid-90s, the performance of 0.1-μm CMOS devices measured by the unity current gain frequency, f_T, was comparable to the highest reported values for BJTs, but at lower power and cost (Taur et al, 1997). Now more than a decade later, conventional CMOS has reached its simple scaling limits. However, unlike the 90s, there is presently no new device to realistically compete with or potentially replace the industry work horse for VLSI applications. Carbon nanotubes and silicon nanowires are considered to be leading contenders but have yet to achieve commercial success in even a niche logic or memory market.

1.2.2 Feature-Enhanced CMOS

In order to meet customer needs for a continuation of Moore's law, feature enhancement instead of simple geometric scaling of the silicon CMOS platform is recognized as the necessary driver for the microelectronics industry. Key features include strain, metal gate, high-κ dielectric, nonplanar geometries, and heterogeneous semiconductor integration. The first key feature to enhance 90, 65, and 45-nm technology nodes is uniaxial process-induced stress (Chan et al, 2003; Murthy et al, 2003; Ghani et al, 2003; Yang et al, 2004) (Chidambaram et al, 2004; Chien-Hao et al, 2004; Liu et al, 2005). Successive features have been added to stress including metal gate and high-κ

dielectric (Mistry et al, 2007; Packan et al, 2008). Instead of increasing the geometrical scaling, future advancements are expected to be an increase in additive feature enhancements.

The development of the first commercial strain feature-enhanced silicon technology is reviewed in (Thompson et al, 2006a). An early question was on the source of the strain: lattice-mismatched epitaxial layers on a fully relaxed substrate or process-induced source/drain stress or intrinsic stress in deposited thin films. Following the promising $Si/Si_{1-x}Ge_x$ heteroepitaxy results, wafer based substrate strain was experimentally and theoretically studied by a large number of researchers (Rim et al 2003, and references therein). In the 90s, two process-induced strain sources were investigated, high stress capping layers deposited on MOSFETs (Shimizu et al, 2001; Ito et al, 2000) and embedded SiGe source and drain (Gannavaram et al, 2000) although the SiGe source and drain was originally proposed for higher boron activation and reduced external resistance. The embedded SiGe literature prompted Intel to evaluate the technology, which resulted in larger than expected device performance enhancement, which after considerable internal debate was later attributed to compressive channel stress (Thompson et al, 2002). However, neither biaxial nor uniaxial stress was immediately adopted in CMOS logic technologies for several reasons (Thompson et al, 2006a). For biaxial stress, issues included defects in the substrate and performance loss at high vertical electric fields (Fischetti et al, 2003). Process-induced uniaxial channel stress was not initially adopted since different stress types (compressive and tensile for n and p-channel respectively) were needed.

After careful analysis of the hole mobility enhancement at high vertical electric fields and the potential for continued effectiveness at nanoscale dimensions, process-induced uniaxial strain was adopted over biaxial stress. Uniaxial stress provided significantly larger hole mobility enhancement at both low strain and high vertical electric field (Thompson et al, 2004b). Since high strain can lead to strain relaxation via defect formation, large mobility enhancement at low strain is critical for yield. Uniaxial stress also provided larger drive current improvement for nanoscale short channel devices since the enhanced electron and hole mobility arises mostly from reduced conductivity effective mass instead of primarily from reduced scattering for biaxial stress. Another important consideration was the strain effect on the threshold voltage. Process-induced uniaxial stress resulted in an approximately five times smaller n-channel threshold voltage shift. The smaller threshold voltage shift was manifested in a smaller penalty for threshold voltage shift retargeting by adjusting the channel doping. Alternately, the larger threshold voltage shift for the substrate-induced biaxial tensile stress causes approximately half of the stress-enhanced electron mobility to be lost (Fossum and Weimin, 2003). Based on the merits of uniaxial stress and the necessity for opposite stress types for n- and p-channel MOSFETs, two process flows were developed that independently targeted the stress magnitude and direction (Thompson et al, 2006b). The first involved embedded and raised SiGe in the p-channel source

and drain and a tensile capping layer on the n-channel device. The second used dual stress liners: compressive and tensile silicon nitride (SiN) for p- and n-channel devices, respectively. As a feature enhancement for CMOS, process-induced stress is employed in nearly all high-performance logic technologies at the 90, 65, and 45-nm technology nodes for both microprocessor and consumer products (Zhang et al, 2005; Bai et al, 2004; Yang et al, 2004; Chan et al, 2003; Thompson et al, 2004a; Qiqing et al, 2005; Ghani et al, 2003; Pidin et al, 2004; Liu et al, 2005; Mistry et al, 2007; Packan et al, 2008).

1.2.3 Variable Strain Sensors

In contrast to the fixed strain incorporated in logic devices for a fixed or constant improvement in device performance, piezoresistive strain sensors respond to variable strain through a modulation in the device resistance. The underlying physics of performance improvement in logic devices and strain transduction in piezoresistive strain sensors is the same. While improvement of logic device performance requires an increase in mobility, which dictates the "sign" of the fixed strain, strain sensors respond to both negative (compressive) and positive (tensile) strains. Since the strain is fixed in logic devices, the linearity of mobility increase with strain is not an issue since the strain is theoretically frozen into the device by stressors incorporated into the device structure during the manufacturing process. In contrast, piezoresistive strain sensors are designed to transduce or detect varying strains by producing a proportional change in resistance. Hence, linear resistance change with strain is important to sense/transduce strains of varying amplitudes into an electrical signal without introducing distortion.

In contrast to discrete strain gauge sensors that are assumed to measure the local strain without significantly affecting the stiffness of the structure in question, integrated stress transducers are devices that integrate the piezoresistive strain gauge within a sensing structure. The combination of MEMS and semiconductor strain gauges has enabled the development of integrated stress transducers. A conventional discrete strain transducer is contrasted with a MEMS piezoresistive pressure stress transducer (microphone) and a fixed stress-enhanced p-channel MOSFET in Fig. 8.13 which is also reproduced as Fig. 1.1 here for an example.

Although it is possible to construct a discrete thin and compliant silicon strain gauge in the same manner as a metal film strain gauge, the vast silicon integrated circuit manufacturing knowledge base coupled with the fortuitous mechanical properties of silicon (Peterson, 1982) has enabled the fabrication of MEMS stress transducers that integrate silicon piezoresistors with a mechanical structure made of the same silicon material.

1.2.4 Strained Quantum Well Optoelectronics

Strain has been an inevitable part of modern heterostructure devices employed in advanced quantum well solid-state lasers and other optoelectronic devices.

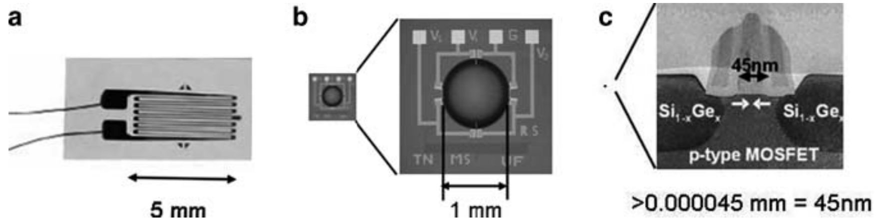

Fig. 1.1. Applications of strain and stress: (**a**) Discrete strain gauge (Omega.com, 2003–2009) (**b**) Si MEMS piezoresistive variable stress transducer with four integrated Si piezoresistors (Arnold et al, 2001) and (**c**) fixed stress enhanced transistor (Thompson et al, 2004a)

While a positive feature enhancement for CMOS, in optoelectronic devices strain was a undesirable by-product from lattice-mismatched semiconductor interfaces, a scourge to be managed in order to avoid quantum efficiency-killing nonradiative defects created by strain relaxation. However, due to improvements in semiconductor film growth technology, strain grading buffer layers, and scaling of device size, strain relaxation is better controlled. With better defect control, strain effects on the band structure offer great potential for enhancing the performance of optoelectronic devices such as solid-state lasers.

Because of the different operation mechanisms, the emphasis of strain effects on band structure is different for optoelectronic devices compared with CMOS. While strain feature enhancement for CMOS is tied primarily to its benefits for electron transport, strain effects on photon emission caused by radiative electron transitions are key for emissive optoelectronic devices. Photon emission is caused by radiative electron transitions in semiconductors such as electron–hole recombination. Since recombination involves two electronic states, the transition probability is determined by the electronic state properties such as energy and wave function. The collective processes of photons, i.e., light emission (as well as absorption), depend on the semiconductor band structure. Strain affects the band structure and thus also affects the performance of optoelectronic devices such as wavelength, gain, linewidth, and quantum efficiency. As will be seen, strain effects on the band structure that affect optoelectronic devices include shifts of the bandgap, changes of energy level density of states (DOS), and electronic wavefunction variation or mixing.

1.3 ORGANIZATION

This book is organized in three major parts. The overall arc of the book follows a trajectory beginning with strain fundamentals for a semiconductor at equilibrium through nonequilibrium transport to strain applications on semiconductor devices.

Part I, "Band Structures of Strained Semiconductors," first reviews stress and strain and crystal symmetry. Strain effects on semiconductors are then introduced by its effects on symmetry. The main physics of interest here that underpins all of the physics of strain is its effects on band structure, which is discussed next initially for an unstrained semiconductor crystal. Strain effects are introduced within two major band structure calculation frameworks, the tight-binding approach and the $\mathbf{k} \cdot \mathbf{p}$ approach. Since the discussion of band structure is originally for a bulk semiconductor, i.e., one that is unconstrained in dimension, the first part finishes with a discussion of the unique differences in the band structure and its strain effects for low-dimensional structures such as a two-dimensional (2D) electron gas such as that created in a MOSFET and a quantum well heterostructure and a one-dimensional nanowire.

Part II, "Transport Theory of Strained Semiconductors," discusses how changes in band structure coupled with changes in carrier scattering caused by strain affect carrier transport. Carrier transport is first reviewed beginning with the Drude model for electron transport in an unstrained semiconductor followed by a qualitative discussion of how strain affects each component of carrier transport. A key transport factor, scattering, is then reviewed by covering the primary scattering processes, lattice, phonon, piezoelectric, and impurity scattering, in a three-dimensional (3D) spatially unconfined structure. Strain effects on the bulk scattering rates are then discussed followed by a discussion of the scattering mechanism unique to spatially confined structures, surface roughness scattering. Finally, the strain effects on carrier transport are summarized in terms of the piezoresistance effect, electron and hole transport, and surface roughness scattering. Strain effects on the high lateral field and near-ballistic transport are also explored.

With the formalities of strain effects on equilibrium and nonequilibrium semiconductors largely discussed, Part III discusses applications of strain to semiconductor devices. Three categories of strain applications are included: (1) fixed strain feature enhancement of electron devices such as Si and SiGe planar and nonplanar MOSFETs, (2) variable strain transducers such as discrete strain gauges and integrated MEMS piezoresistive stress transducers, and (3) optoelectronic devices where strain is a by-product of the quantum well heterostructures employed and an effect to be managed as well as exploited.

Part I

Band Structures of Strained Semiconductors

2

Stress, Strain, Piezoresistivity, and Piezoelectricity

2.1 STRAIN TENSOR

Strain in crystals is created by deformation and is defined as relative lattice displacement. For simplicity, we use a 2D lattice model in Fig. 2.1 to illustrate this concept, but discuss the general concept in 3D cases. As shown in Fig. 2.1a, we may use two unit vectors $\hat{x}$, $\hat{y}$ to represent the unstrained lattice, and in a simple square lattice, they correspond to the lattice basis vectors. Under a small uniform deformation of the lattice, the two vectors are distorted in both orientation and length, which is shown in Fig. 2.1b. The new vectors $\hat{\mathbf{x}}'$ and $\hat{\mathbf{y}}'$ may be written in terms of the old vectors:

$$\hat{\mathbf{x}}' = (1 + \varepsilon_{xx})\hat{x} + \varepsilon_{xy}\hat{y} + \varepsilon_{xz}\hat{z}, \tag{2.1}$$

$$\hat{\mathbf{y}}' = \varepsilon_{yx}\hat{x} + (1 + \varepsilon_{yy})\hat{y} + \varepsilon_{yz}\hat{z}, \tag{2.2}$$

and in the 3D case, we also have

$$\hat{\mathbf{z}}' = \varepsilon_{zx}\hat{x} + \varepsilon_{zy}\hat{y} + (1 + \varepsilon_{zz})\hat{z}. \tag{2.3}$$

The strain coefficients $\varepsilon_{\alpha\beta}$ define the deformation of the lattice and are dimensionless. The 3×3 matrix

$$\bar{\bar{\varepsilon}} = \begin{pmatrix} \varepsilon_{xx} & \varepsilon_{xy} & \varepsilon_{xz} \\ \varepsilon_{yx} & \varepsilon_{yy} & \varepsilon_{yz} \\ \varepsilon_{zx} & \varepsilon_{zy} & \varepsilon_{zz} \end{pmatrix} \tag{2.4}$$

is called the strain tensor. A tensor is a mathematical notation, usually represented by an array, to describe a linear relation between two physical quantities. A tensor can be a scalar, a vector, or a matrix. A scalar is a zero-rank tensor, a vector is a first-rank tensor, and a matrix is a second-rank tensor, and so on. The strain tensor is a second-rank tensor, which in this book is labeled with two bars over the head. However, in places without confusion, we usually neglect the bars. Suppose a lattice point is originally located

Y. Sun et al., *Strain Effect in Semiconductors: Theory and Device Applications*, DOI 10.1007/978-1-4419-0552-9_2,
© Springer Science+Business Media, LLC 2010

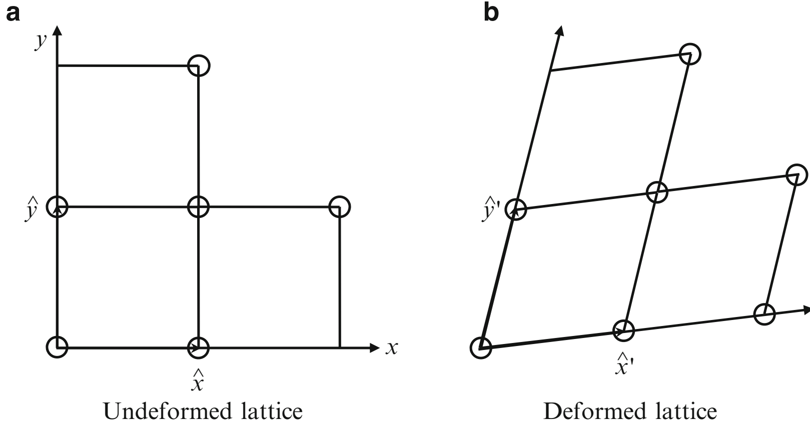

Fig. 2.1. Diagram for (**a**) an undeformed lattice and (**b**) a deformed lattice

at $\mathbf{r} = x\hat{x} + y\hat{y} + z\hat{z}$, then with a uniform deformation this point will be at $\mathbf{r}' = x\hat{\mathbf{x}}' + y\hat{\mathbf{y}}' + z\hat{\mathbf{z}}'$. For a general varying strain, the strain tensor may be written as

$$\varepsilon_{\alpha,\beta} = \frac{\partial u_\alpha}{\partial x_\beta}, \qquad u_\alpha = u_x, u_y, u_z,\ x_\beta = x, y, z, \tag{2.5}$$

where u_α is the displacement of lattice point under study along x_α. A strain tensor (2.4) is symmetric, i.e.,

$$\varepsilon_{\alpha\beta} = \varepsilon_{\beta\alpha} = \frac{1}{2}\left(\frac{\partial u_\alpha}{\partial x_\beta} + \frac{\partial u_\beta}{\partial x_\alpha}\right). \tag{2.6}$$

The antisymmetric part of tensor (2.4) represents a rotation of the entire body.

Usually people work with the other set of strain components, which are defined as

$$e_{xx} = \varepsilon_{xx}; \quad e_{yy} = \varepsilon_{yy}; \quad e_{zz} = \varepsilon_{zz}, \tag{2.7}$$

which describe infinitesimal distortions associated with a change in volume, and the other strain components e_{xy}, e_{yz}, and e_{zx} are defined in terms of changes of angle between the basis vectors. Neglecting the terms of order ε^2 in the small strain approximation, they are

$$\begin{aligned} e_{xy} &= \hat{\mathbf{x}}' \cdot \hat{\mathbf{y}}' = \varepsilon_{xy} + \varepsilon_{yx}, \\ e_{yz} &= \hat{\mathbf{y}}' \cdot \hat{\mathbf{z}}' = \varepsilon_{yz} + \varepsilon_{zy}, \\ e_{zx} &= \hat{\mathbf{z}}' \cdot \hat{\mathbf{x}}' = \varepsilon_{zx} + \varepsilon_{xz}. \end{aligned} \tag{2.8}$$

These six coefficients completely define the strain. We can write these six strain coefficients in the form of an array as $\mathbf{e} = \{e_{xx}, e_{yy}, e_{zz}, e_{yz}, e_{zx}, e_{xy}\}$. The introduction of this set of notation for the strain components is merely for the convenience of describing the relations between strain and the other strain-related physical quantities. The relation between two second-rank tensors

must be described by a fourth-rank tensor, which is very complicated; while after transforming the second-rank tensors to first-rank, only a second-rank tensor is required.

The crystal dilation under deformation can be evaluated through calculating the volume defined by $\hat{\mathbf{x}}'$, $\hat{\mathbf{y}}'$, and $\hat{\mathbf{z}}'$,

$$V' = \hat{\mathbf{x}}' \cdot \hat{\mathbf{y}}' \times \hat{\mathbf{z}}' = 1 + e_{xx} + e_{yy} + e_{zz}, \tag{2.9}$$

and the dilation δ then is given by

$$\delta = \frac{\delta V}{V} = e_{xx} + e_{yy} + e_{zz}, \tag{2.10}$$

which is the trace of the strain tensor. The dilation is negative for hydrostatic pressure.

2.2 STRESS TENSOR

Crystal deformations can be induced by externally applied forces, or in other words, a solid resists deformations, thus deformations will generate forces. Stress is defined as the force in response to strain in a unit area. Stress has nine components and is a second-rank tensor, which we write as $\tau_{\alpha\beta}$, $\alpha, \beta = x, y, z$. On the surface of an infinitesimal volume cube, the stress distribution is illustrated in Fig. 2.2, where τ_{xx} represents a force applied in the x direction to a unit area of the plane whose outward-drawn normal lies in the x direction, and τ_{xy} represents a force applied in the x direction to a unit area of the

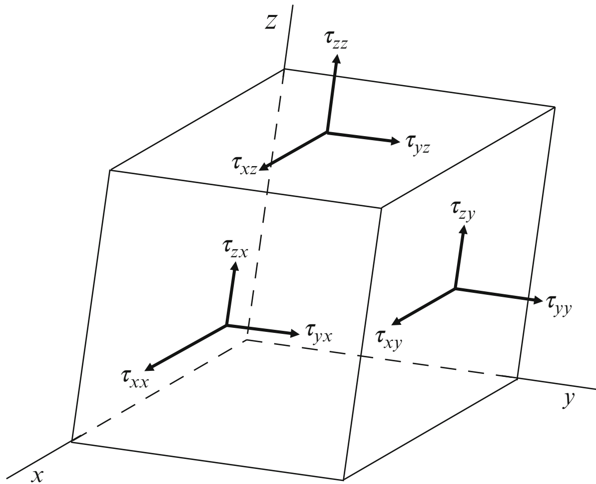

Fig. 2.2. Illustration for stress components on the surfaces of an infinitesimal cube

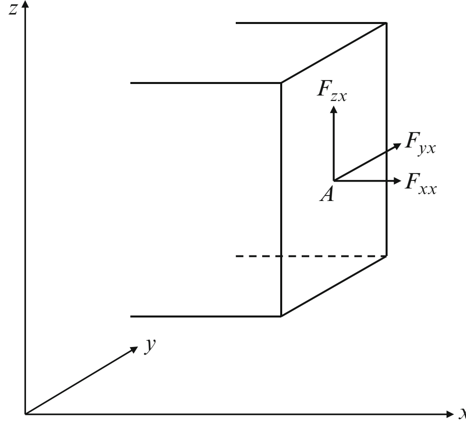

Fig. 2.3. Illustration of the forces applied on one surface with area of A of the cube shown in Fig. 2.2

plane whose outward-drawn normal lies in the y direction. The stress tensor is symmetric just as the strain tensor. The antisymmetric part of the stress tensor represents a torque, and in a state of equilibrium, all torques must vanish inside a solid.

The stress and force relation is better illustrated in Fig. 2.3 where we show a force applied on an infinitesimal plane whose normal is along x and has an area A. In such a case, we resolve the force into components along the coordinate axes, i.e., F_{xx}, F_{yx}, and F_{zx}. The stress components in this plane are

$$\tau_{xx} = \frac{F_{xx}}{A}, \; \tau_{yx} = \frac{F_{yx}}{A}, \; \tau_{zx} = \frac{F_{zx}}{A}. \tag{2.11}$$

We now study some simple stress cases to determine the stress tensors.

1. Hydrostatic pressure:
   Under a hydrostatic pressure P, all shear stress is zero. Stress along any principle direction is $-P$, namely,
   $$\tau = \begin{pmatrix} -P & 0 & 0 \\ 0 & -P & 0 \\ 0 & 0 & -P \end{pmatrix}. \tag{2.12}$$
   Here the sign convention is that tensile stress is positive and compressive stress is negative.
2. Uniaxial stress T along the [001] direction:
   For a uniaxial stress T along the [001] direction, all stress components but τ_{zz} are zero, and $\tau_{zz} = T$. So
   $$\tau = \begin{pmatrix} 0 & 0 & 0 \\ 0 & 0 & 0 \\ 0 & 0 & T \end{pmatrix}. \tag{2.13}$$

3. Uniaxial stress T along the [110] direction:
   The case for a uniaxial stress along the [110] direction is a little more complicated. Generally when we talk about a stress T along the $\langle 110 \rangle$ direction, it refers to the force exerted along the $\langle 110 \rangle$ direction divided by the cross section of the (110) surface, but not necessarily equal to any of the stress tensor elements. To find the stress elements, we can use two methods. First is to resolve the force into three coordinate axes. For [110] uniaxial stress T as shown in Fig. 2.4a, the force along the [110] direction is $F = Ta^2$. Its component along [001] is zero. Along both x and y direction, the force is $F/\sqrt{2}$. However, the cross area for the force along [110] shown in Fig. 2.4a is a^2 and is $\sqrt{2}a^2$ for the forces along the x and y direction. Thus, the stress along both x and y is $F/2a^2 = T/2$. The shear stress on both [100] and [010] planes is also $T/2$. The second method to obtain the stress components is through the coordinate transformation method. Suppose in an unprimed coordinate system, stress T is along the x direction, and thus $\tau_{xx} = T$, and all the other stress components are zero. We can rotate the x and y axes 45° clockwise, and then an original [100] uniaxial stress that only has one nonvanishing component $\tau_{xx} = T$ now corresponds to a [110] uniaxial stress in a primed coordinate system, as shown in Fig. 2.4b. The stress elements in the primed coordinate system are given by the transformation,

$$\tau'_{ij} = \sum_{mn} \tau_{mn} \frac{\partial x'_i}{\partial x_m} \frac{\partial x'_j}{\partial x_n}, \tag{2.14}$$

where $\frac{\partial x'_i}{\partial x_m}$, etc. represent the directional cosines of the transformed axes made to the original axes. This equation results from the general tensor transformation of S to S' under an orthogonal coordinate transformation A,

$$S' = ASA^{\mathrm{T}}, \tag{2.15}$$

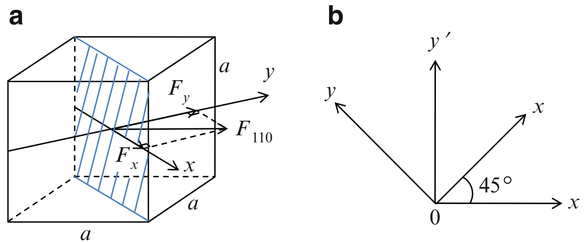

Fig. 2.4. (**a**) The decomposition of a force along the [110] direction along the x and y directions, and their stress relations. Please note that in this figure, the x and y directions are along the diagonals of the surfaces instead of along the edges. (**b**) The coordinate systems before and after a 45° rotation clockwise. The unprimed and primed systems are the coordinate systems before and after the rotation

where A^{T} is the transpose of matrix A. The stress tensor under the [110] uniaxial stress found using both methods is

$$\tau = \frac{\mathrm{T}}{2}\begin{pmatrix} 1 & 1 & 0 \\ 1 & 1 & 0 \\ 0 & 0 & 0 \end{pmatrix}. \tag{2.16}$$

Because a stress tensor is symmetric, similar to the strain tensor case, the six coefficients, τ_{xx}, τ_{yy}, τ_{zz}, τ_{yz}, τ_{zx}, and τ_{xy} completely define the stress. Similar to a strain tensor, a second-rank stress tensor can be reduced to a 1D array form.

2.3 ELASTIC COMPLIANCE AND STIFFNESS CONSTANTS

In the linear elastic theory, Hooke's law is justified and stress is proportional to strain

$$\tau_{ij} = \sum_{\alpha\beta} C_{ij\alpha\beta} e_{\alpha\beta}, \quad i, j, \alpha, \beta = x, y, z, \tag{2.17}$$

where the coefficients $C_{ij\alpha\beta}$ are called elastic stiffness constants. Elastic stiffness constants are a fourth-rank tensor. Because of the symmetry of both the strain tensor and the stress tensor, we have

$$C_{ij\alpha\beta} = C_{ji\alpha\beta} = C_{ij\beta\alpha}, \tag{2.18}$$

so we may write both strain and stress tensor as a six-component array as

$$\mathbf{e} = (e_{xx}, e_{yy}, e_{zz}, e_{yz}, e_{zx}, e_{xy}) \tag{2.19}$$

and

$$\tau = (\tau_{xx}, \tau_{yy}, \tau_{zz}, \tau_{yz}, \tau_{zx}, \tau_{xy}) \tag{2.20}$$

and reduce the elastic stiffness tensor to a 6×6 matrix

$$\tau_i = \sum_m C_{im} e_m. \tag{2.21}$$

This 6×6 matrix has a very simple form in cubic crystals due to the high symmetry. It has only three independent components and has the form

$$C_{ij} = \begin{pmatrix} C_{11} & C_{12} & C_{12} & 0 & 0 & 0 \\ C_{12} & C_{11} & C_{12} & 0 & 0 & 0 \\ C_{12} & C_{12} & C_{11} & 0 & 0 & 0 \\ 0 & 0 & 0 & C_{44} & 0 & 0 \\ 0 & 0 & 0 & 0 & C_{44} & 0 \\ 0 & 0 & 0 & 0 & 0 & C_{44} \end{pmatrix}. \tag{2.22}$$

This is easy to understand by inspecting (2.21) and considering the transformation of this equation under symmetry operations. First, the elastic stiffness tensor must be symmetric. Second, since for cubic crystals, the three axes are equivalent, therefore we must have $C_{11} = C_{22} = C_{33}$, and $C_{44} = C_{55} = C_{66}$. Third, a shear strain cannot cause a normal stress, so terms like $C_{14} = 0$. And a shear strain along one axis cannot induce forces causing a shear along another axis, so terms like $C_{45} = 0$. Finally in the view of a force along one axis, the other two axes are equivalent, and thus we have $C_{12} = C_{13}$, etc. These results can also be obtained by investigating the transformation of the components in (2.17) under symmetry operations using an equation similar to (2.14)

$$C'_{lk\gamma\delta} = \sum_{ij\alpha\beta} C_{ij\alpha\beta} \frac{\partial x'_l}{\partial x_i} \frac{\partial x'_k}{\partial x_j} \frac{\partial x'_\gamma}{\partial x_\alpha} \frac{\partial x'_\delta}{\partial x_\beta}. \tag{2.23}$$

For example, it is easy to verify that under a reflection and thus $x \to -x$, $C_{xyzz} = -C_{xyzz}$, so in the 6×6 matrix, $C_{63} = 0$.

In many cases it is convenient to work with the inverse of the elastic stiffness tensor, which is defined through the relation between strain and stress

$$\varepsilon_{\alpha\beta} = \sum_{ij} S_{\alpha\beta ij} \tau_{ij}. \tag{2.24}$$

The fourth-rank tensor $S_{\alpha\beta ij}$, called the compliance tensor, can also be reduced into a 6×6 matrix. Under cubic symmetry, it has the same form as the stiffness tensor

$$\begin{pmatrix} S_{11} & S_{12} & S_{12} & 0 & 0 & 0 \\ S_{12} & S_{11} & S_{12} & 0 & 0 & 0 \\ S_{12} & S_{12} & S_{11} & 0 & 0 & 0 \\ 0 & 0 & 0 & S_{44} & 0 & 0 \\ 0 & 0 & 0 & 0 & S_{44} & 0 \\ 0 & 0 & 0 & 0 & 0 & S_{44} \end{pmatrix}, \tag{2.25}$$

and the strain–stress relation can be written as

$$e_m = \sum_i S_{mi} \tau_i. \tag{2.26}$$

Because the elastic stiffness tensor and compliance tensor are inverse to each other, so it is easy to work out the relations between the components as

$$\begin{aligned} S_{11} &= \frac{C_{11} + C_{12}}{(C_{11} - C_{12})(C_{11} + 2C_{12})}, \\ S_{12} &= \frac{-C_{12}}{(C_{11} - C_{12})(C_{11} + 2C_{12})}, \\ S_{44} &= \frac{1}{C_{44}}. \end{aligned} \tag{2.27}$$

In mechanical engineering, Young's modulus Y and Poisson ration ν are commonly used. For a homogeneous, isotropic material, strain is related to stress through

$$\begin{aligned}\varepsilon_{xx} &= \frac{1}{Y}(\tau_{xx} - \nu(\tau_{yy} + \tau_{zz})),\\ \varepsilon_{yy} &= \frac{1}{Y}(\tau_{yy} - \nu(\tau_{zz} + \tau_{xx})),\\ \varepsilon_{zz} &= \frac{1}{Y}(\tau_{zz} - \nu(\tau_{xx} + \tau_{yy})).\end{aligned} \tag{2.28}$$

In cubic systems Young's modulus and Poisson ration ν are related to the compliance constants by

$$Y = \frac{1}{S_{11}},\ \nu = -\frac{S_{12}}{S_{11}}. \tag{2.29}$$

2.4 EXAMPLES OF STRESS–STRAIN RELATIONS

Now we use two examples to illustrate how to determine the strain tensor from stress using the relations we have discussed earlier.

1. Biaxial stress:
   A semiconductor layer pseudomorphically grown on a (001)-oriented lattice-mismatched substrate is schematically shown in Fig. 2.5. In this case, the top layer is biaxially strained, and the strain components e_{xx} and e_{yy} are

$$e_{xx} = e_{yy} = \frac{a_0 - a}{a}. \tag{2.30}$$

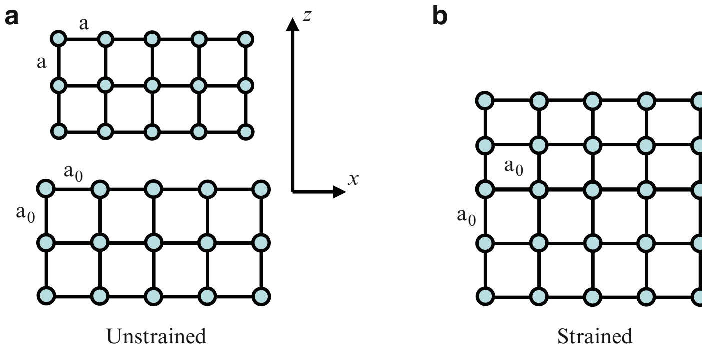

Fig. 2.5. Illustration of biaxial stress (strain). (**a**) Two different material layers have different lattice constant before growth; (**b**) After pseudomorphic film growth, the lattice constant of the top layer conforms to that of the bottom layer and is under biaxial stress (strain)

The strain is tensile in the x-y plane. To obtain the strain in the z direction, we use the strain–stress relation (2.26), i.e.,

$$\begin{bmatrix} e_{xx} \\ e_{yy} \\ e_{zz} \\ e_{zx} \\ e_{yz} \\ e_{xy} \end{bmatrix} = \begin{bmatrix} S_{11} & S_{12} & S_{12} & 0 & 0 & 0 \\ S_{12} & S_{11} & S_{12} & 0 & 0 & 0 \\ S_{12} & S_{12} & S_{11} & 0 & 0 & 0 \\ 0 & 0 & 0 & S_{44} & 0 & 0 \\ 0 & 0 & 0 & 0 & S_{44} & 0 \\ 0 & 0 & 0 & 0 & 0 & S_{44} \end{bmatrix} \begin{bmatrix} \tau_{xx} \\ \tau_{yy} \\ \tau_{zz} \\ \tau_{zx} \\ \tau_{yz} \\ \tau_{xy} \end{bmatrix} . \tag{2.31}$$

In the current case, $\tau_{xx} = \tau_{yy} = T$, $\tau_{zz} = 0$, and $\tau_{zx} = \tau_{yz} = \tau_{xy} = 0$. Therefore, we have

$$\begin{aligned} e_{xx} &= e_{yy} = (S_{11} + S_{12})T, \\ e_{zz} &= 2S_{12}T. \end{aligned} \tag{2.32}$$

Thus,

$$e_{zz} = \frac{2S_{12}}{S_{11} + S_{12}} e_{xx}. \tag{2.33}$$

Strain tensor in this case is

$$e = \begin{pmatrix} e_{xx} & 0 & 0 \\ 0 & e_{xx} & 0 \\ 0 & 0 & e_{zz} \end{pmatrix} . \tag{2.34}$$

2. [110] uniaxial stress:
   The x-y plane of a cubic crystal under a [110] uniaxial stress is illustrated in Fig. 2.6. The stress tensor is already obtained in Eq. (2.16), i.e., $\tau_{xx} = \tau_{yy} = \tau_{xy} = T/2$, and $\tau_{zz} = \tau_{zx} = \tau_{yz} = 0$. Substituting into (2.31), we obtain

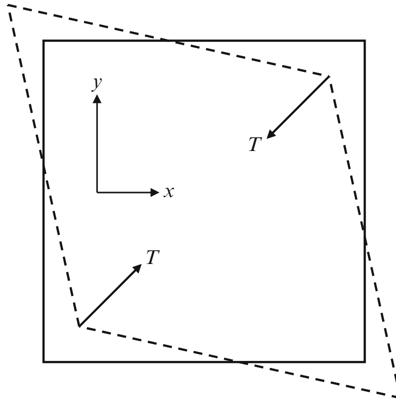

Fig. 2.6. Illustration of the [110] uniaxial compressive stress (strain)

$$
\begin{aligned}
e_{xx} &= e_{yy} = \frac{S_{11}+S_{12}}{2}T, \\
e_{xy} &= \frac{S_{44}}{2}T, \\
e_{zz} &= S_{12}T.
\end{aligned}
\tag{2.35}
$$

The strain tensor in this case then is

$$
\varepsilon = \begin{pmatrix} e_{xx} & e_{xy}/2 & 0 \\ e_{xy}/2 & e_{xx} & 0 \\ 0 & 0 & e_{zz} \end{pmatrix}. \tag{2.36}
$$

2.4.1 Hydrostatic and Shear Strain

An arbitrary strain tensor can be decomposed into three separate tensors as following:

$$
\begin{aligned}
\begin{pmatrix} \varepsilon_{xx} & \varepsilon_{xy} & \varepsilon_{xz} \\ \varepsilon_{yx} & \varepsilon_{yy} & \varepsilon_{yz} \\ \varepsilon_{zx} & \varepsilon_{zy} & \varepsilon_{zz} \end{pmatrix} &= \frac{1}{3}\begin{pmatrix} \varepsilon_{xx}+\varepsilon_{yy}+\varepsilon_{zz} & 0 & 0 \\ 0 & \varepsilon_{xx}+\varepsilon_{yy}+\varepsilon_{zz} & 0 \\ 0 & 0 & \varepsilon_{xx}+\varepsilon_{yy}+\varepsilon_{zz} \end{pmatrix} \\
&+ \frac{1}{3}\begin{pmatrix} 2\varepsilon_{xx}-(\varepsilon_{yy}+\varepsilon_{zz}) & 0 & 0 \\ 0 & 2\varepsilon_{yy}-(\varepsilon_{zz}+\varepsilon_{xx}) & 0 \\ 0 & 0 & 2\varepsilon_{zz}-(\varepsilon_{xx}+\varepsilon_{yy}) \end{pmatrix} \\
&+ \begin{pmatrix} 0 & \varepsilon_{xy} & \varepsilon_{xz} \\ \varepsilon_{yx} & 0 & \varepsilon_{yz} \\ \varepsilon_{zx} & \varepsilon_{zy} & 0 \end{pmatrix},
\end{aligned}
\tag{2.37}
$$

where the first constant tensor whose diagonal element is one-third of the trace of the original strain tensor accounts for the volume change [see (2.10)], and the latter two traceless tensors account for the shape change of an infinitesimal cube. Correspondingly, the first tensor describes the effect of a hydrostatic strain, and the latter two tensors describe the effect of shear strain. Among the two shear strain tensors, the diagonal one is related to the change of lengths along the three axes and the other one with diagonal elements being zero is related to the rotation of the axes of an infinitesimal cube. For a cubic crystal, the first type of shear occurs when a uniaxial stress is applied along any of the three $\langle 100\rangle$ axes, and the second type of shear is nonzero only when stresses are applied along $\langle 110\rangle$ or $\langle 111\rangle$ axes. Obviously, for a cube under the hydrostatic strain, the shape does not change, while under an arbitrary first type of shear, the shape of the cube will become orthorhombic, and under an arbitrary second type of shear, the shape of the cube will become triclinic. A cubic crystal under biaxial stress becomes tetragonal, and it becomes orthorhombic under a uniaxial stress along $\langle 110\rangle$.

For a first look, applying a compressive uniaxial stress along [001] and a biaxial tensile stress in the x-y plane to a cubic crystal seems identical. Indeed, if for both cases the stress is T, and we decompose the resulting strain tensor into the hydrostatic and shear parts, the shear strain coincides. However, the hydrostatic strain differs in sign and a factor of 2 in magnitude.

2.5 PIEZORESISTIVITY

Piezoresistivity is an effect of stress-induced resistivity change of a material. The piezoresistance coefficients (π coefficients) that relate the piezoresistivity and stress are defined by

$$\pi = \frac{\Delta R/R}{T}, \tag{2.38}$$

where R is the original resistance that is related to semiconductor sample dimension by $R = \rho\frac{l}{wh}$, ΔR signifies the change of resistance, and T is the applied mechanical stress. The ratio of ΔR to R can be expressed in terms of relative change of the sample length $\Delta l/l$, width $\Delta w/w$, height $\Delta h/h$, and resistivity $\Delta\rho/\rho$ as

$$\frac{\Delta R}{R} = \frac{\Delta l}{l} - \frac{\Delta w}{w} - \frac{\Delta h}{h} + \frac{\Delta\rho}{\rho}, \tag{2.39}$$

where resistivity ρ is inversely proportional to the conductivity. The first three terms of the RHS of (2.39) depict the geometrical change of the sample under stress, and the last term $\Delta\rho/\rho$ is the resistivity dependence on stress. For most semiconductors, the stress-induced resistivity change is several orders of magnitude larger than the geometrical change-induced resistance change, so the resistivity change by stress is the determinant factor of the piezorestivity.

In general conditions, resistivity $\rho = 1/\sigma$ is a second-rand tensor, and stress T is also a second-rank tensor. The resistivity change, $\Delta\rho_{ij}$, is connected to stress by a fourth-rank tensor π_{ijkl}, the piezoresistance tensor. Under arbitrary stress in linear response regime,

$$\frac{\Delta\rho_{ij}}{\rho} = -\frac{\Delta\sigma_{ij}}{\sigma} = \sum_{k,l} \pi_{ijkl}\tau_{kl}, \tag{2.40}$$

where summation is over x, y, and z.

Following the same discussion for compliance and stiffness tensor, and writing $\Delta\rho_{ij}$ to a vector form $\Delta\rho_i$, where $i = 1, 2, \ldots, 6$, as we did for stress and strain, we can rewrite (2.40) as

$$\frac{\Delta\rho_i}{\rho} = \sum_{k=1}^{6} \pi_{ik}\tau_k, \tag{2.41}$$

where π_{ik} is a 6×6 matrix. For cubic structures, it has only three independent elements due to the cubic symmetry,

$$\pi_{ik} = \begin{pmatrix} \pi_{11} & \pi_{12} & \pi_{12} & 0 & 0 & 0 \\ \pi_{12} & \pi_{11} & \pi_{12} & 0 & 0 & 0 \\ \pi_{12} & \pi_{12} & \pi_{11} & 0 & 0 & 0 \\ 0 & 0 & 0 & \pi_{44} & 0 & 0 \\ 0 & 0 & 0 & 0 & \pi_{44} & 0 \\ 0 & 0 & 0 & 0 & 0 & \pi_{44} \end{pmatrix} . \tag{2.42}$$

Among the three independent π-coefficients, π_{11} depicts the piezoresistive effect along one principal crystal axis for stress along this principal crystal axis (longitudinal piezoresistive effect), π_{12} depicts the piezoresistive effect along one principal crystal axis for stress directed along one perpendicular crystal axis (transverse piezoresistive effect), and π_{44} describes the piezoresistive effect on an out-of-plane electric field by the change of the in-plane current induced by in-plane shear stress.

The detailed discussion of semiconductor piezoresistivity will be covered in Chap. 5.

2.6 PIEZOELECTRICITY

Different from the piezoresistive effect, the piezoelectric effect arises from stress-induced charge polarization in a crystal that lacks a center of inversion. Thus, the piezoelectric effect does not exist in Si, Ge, etc. elementary semiconductors. The zinc-blende semiconductors are the simplest crystals with this property. The polarization is related to stress through the piezoelectric tensor $\bar{\bar{e}}$,

$$\mathbf{P} = [e]\mathbf{e}_{\mathrm{strain}}, \tag{2.43}$$

where $\mathbf{P}$ is the polarization vector and $\mathbf{e}_{\mathrm{strain}}$ is the strain written as a six-component vector. Thus the piezoelectric tensor is a 3×6 matrix. For zinc-blende semiconductors, the piezoelectric tensor only has one nonvanishing tensor element, e_{14}, and the polarization induced by strain is then given by

$$\begin{pmatrix} P_x \\ P_y \\ P_z \end{pmatrix} = \begin{pmatrix} 0 & 0 & 0 & e_{14} & 0 & 0 \\ 0 & 0 & 0 & 0 & e_{14} & 0 \\ 0 & 0 & 0 & 0 & 0 & e_{14} \end{pmatrix} \begin{pmatrix} e_{xx} \\ e_{yy} \\ e_{zz} \\ e_{yz} \\ e_{zx} \\ e_{xy} \end{pmatrix} . \tag{2.44}$$

Because of the special form of the piezoelectric tensor, only the shear strain generates the piezoelectricity. For zinc-blende semiconductors such as GaAs grown on (001) direction, the biaxial strain does not generate piezoelectricity.

The piezoelectric effect is largest along the $\langle 111 \rangle$ axes, since the anions and cations are stacked in the (111) planes, thus strain creates relative displacement between them.

The piezoelectric constants of GaAs were measured and theoretically calculated (Adachi, 1994). The commonly adopted value is

$$e_{14} = -0.16 \ \ \mathrm{C/m^2}. \tag{2.45}$$

On the other hand, the applied electric field across the piezoelectric material can generate strain. The piezoelectric strain tensor $\bar{\bar{d}}$ has the same form as the piezoelectric tensor and also has only one nonvanishing component, d_{14}, for zinc-blende semiconductors. It is related to e_{14} by

$$d_{14} = S_{44} e_{14}. \tag{2.46}$$

The commonly adopted value for d_{14} for GaAs is -2.7×10^{-12} m/V.

The sign of e_{14} or d_{14} is negative for III–V semiconductors. If the crystal is expanded along the $\langle 111 \rangle$ direction, the A-faces (cation faces) becomes negatively charged. This is different from the II–V semiconductors, where e_{14} is positive.

For the other semiconductors lacking inversion symmetry, the piezoelectric tensor may have more than one nonvanishing component. In wurtzite semiconductors such as GaN, there are three nonvanishing components, e_{13}, e_{33}, and e_{15}. Piezoelectric effect may play an important role in semiconductor transport. In an AlGaN/GaN heterostructure, the spontaneous polarization and the piezoelectric effect can induce large density of electrons even when there is no doping (Bernardini and Fiorentini, 1997; Jogai, 1998; Sacconi et al, 2001). In GaAs/InGaAs superlattices grown in the $\langle 111 \rangle$ direction, piezoelecticity induced band bending can greatly change the potential profile, and thus alter the charge distribution and transport properties (Smith and Mailhiot, 1988; Kim, 2001).